Journal of Applied Fluid Mechanics, Vol. 18, No. 2, pp. 468-484, 2025.
Available online at www.jafmonline.net, ISSN 1735-3572, EISSN 1735-3645.
https://doi.org/10.47176/jafm.18.2.2735

Multiphase Flow Simulations to Explore Novel Technique of Air Injection to Mitigate Silt Erosion in Hydro Turbines

P. Dhiman, A. Bhat and A. Karn†

Multi Phase Flow Laboratory, Mechanical Cluster, School of Advanced Engineering, UPES, Dehradun, Uttarakhand, India

†Corresponding Author Email: akarn@ddn.upes.ac.in

ABSTRACT

Hydropower is increasingly recognized as a sustainable energy source due to its minimal environmental impact, a crucial factor in meeting global energy demands. However, the efficiency of hydropower plants (particularly in the Himalayan region) can be hampered by wear and tear of essential components like hydroturbine blades, runners, guide vanes, and nozzles, caused by silt particles in water streams. This study proposes an innovative solution to mitigate silt erosion by implementing a partial air shield on the pressure surface of hydrofoils. Through numerical simulations, the study investigates the interaction between quartz particle-water suspension and injected air on a NACA 4412 hydrofoil. The Euler-Euler-Lagrange model combined with the *K*-omega SST turbulence scheme is observed to accurately predict erosion wear behavior with and without air injection. The investigation reveals two significant phases. Initially, a comparison between scenarios with and without air injection shows a noticeable reduction in erosion rate when air is introduced over the surface. To further illustrate this reduction, the study increases the silt suspension levels from 2500 ppm to 5000 ppm and the air injection speed from 7.5 m/s to 17.5 m/s, while maintaining a constant hydrofoil angle of attack at 10° and an air-injection angle of 30°. In the subsequent phase, detailed exploration of various air injection parameters reveals an inverse relationship between air injection speed and erosion rate. This study provides comprehensive data sheets illustrating results for different parameter ranges, suggesting that air entrainment on hydroturbine runners can effectively reduce wear due to silt.

Article History

Received March 31, 2024
Revised July 9, 2024
Accepted August 29, 2024
Available online December 4, 2024

Keywords:

Silt erosion
Hydro turbines
Air injection
Erosion mitigation
Cavitation

1. INTRODUCTION

Energy has a significant impact on the sustainable development of a country. Per capita energy consumption is always rising, driven by the ongoing processes of industrialization and urbanization in both developed and developing nations. The need for renewable energy has significantly increased recently due to factors such as expanding energy reliance, rising global energy demand, environmental concerns related to fuel usage, and volatile fossil fuel costs. The increasing need to address issues like poverty, pollution, health problems, and environmental degradation has caused this spike in the demand for renewable energy (Shahsavari & Akbari, 2018). Hydropower has a number of advantages over conventional-based power generation resources, but some problems with these power generation houses hinder power production. Problems like cavitation, erosion, corrosion, vibration, imbalance, and mechanical breakdowns, which not only increase the downtime of the facility but also increase the overall cost of power generation.

Sediment erosion is one of the leading causes of failure and downtime for hydro-turbine plants situated in the Himalayan and Uttarakhand regions of India and mostly envelops the Indus, the Brahmaputra, and the Ganga drainage basins. Turbine blades are the worst-affected element within the entire hydro-turbine setup and are prone to aggravated damage during the peak monsoon when sediment transport increases up to 20,000 ppm (Masoodi & Harmain, 2017). Also, Thapa et al. (2015) has reported about

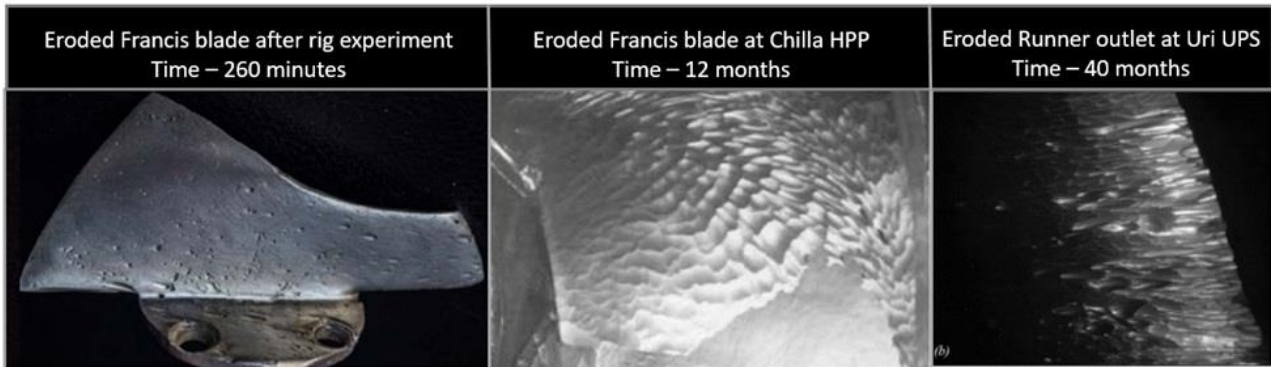

Fig. 1 Erosion wear damage results on Francis blade. Left to Right: Adapted from Masoodi and Harmain (2017); Rajkarnikar et al. (2013) and Sangal et al. (2018), respectively

the loss in turbine hydraulic efficiency and its operating reliability due to slit erosion. For instance, the working efficiency of the turbine decreased by 2.38 and 4.97 percent under full and half loading conditions respectively, for a single monsoon season (year 2008-2009) at the Manari Bhali project (Singh et al., 2013). A similar case was reported in Nepal in 2003, when 69,000 tons of sediment flow was recorded for a mere three-month span, with a reduction in efficiency estimated at 4.0 and 8.0 percent for the full and half load conditions respectively (Man & Pradhan, 2004). Further, Uri and Dulhasti power stations in Jammu and Kashmir are considered among the 'extensive damage' regions, with runner requiring maintenance in as short as one year. Furthermore, Fig. 1 represents the intensity of damage to the Francis turbine blade for various time intervals located at different locations in India.

Although, Padhy and Saini (2008) after performing an extensive review of theoretical and experimental investigations, suggested that only reductions in silt erosion can be obtained not the complete eradication of silt erosion. However, Thapa et al. (2012) emphasizes the optimization of the geometrical characteristics of a Francis runner blade to attenuate the erosion effect by about 30 percent, but this is widely contradicted as it accelerates pitting in the guide vane region. Similarly, Teran et al. (2016) proposed a trade-off that demonstrated a total reduction in erosion by 39 percent at the cost of losing overall efficiency by 5 percent using a modified flow distribution channel.

Thereafter, further studies pointed that the intensity of erosion over a turbine blade relies on several governing factors, such as the shape and size of silt particles, silt constituents and their hardness, particle impingement velocity, particle incident angle during the impact, particle concentration, frequency of particle-blade interaction, blade material, blade profile, and the operational angle of attack (Hua et al., 2015; Peng & Cao, 2016). The presence of extremely hard mineral (quartz) particles having a hardness between 5-7 on Mohr's scale usually forms an aggregate of 50 to 98 percent of the total silt concentration in a stream (Masoodi & Harmain, 2017; Acharya et al., 2019). Such high concentrations elevate the deterioration process, which is also relatively dependent on the net volume flow rate of the sediment-water mixture. The relationship between particle velocity and erosion suggested by Truscott (1972) recommended that the erosion rate is directly proportional to the velocity power law. The constitutive relationship can be expressed as: Rate of erosion $\propto V^{n}$, where the exponent 'n' is reported to be in a range of 3-4 for a state of pure erosion (Kang et al., 2016). Moreover, an experimental study evaluating the effect of sharp and blunt particle shapes on wear was characterized by Bahadur and Badruddin (1990). Values of 1, 0.53 and 0.2, correspond to triangular, semi-spherical and spherical shapes that are used during calculations. Usually, the largest sediment particles are expected in the upstream region when compared to the later stages in the downstream region. Having said that, the same is not always true but is location sensitive. In a similar way, high flow rates arising due to unpredictable seasonal transitions often increase the quantity of large sediment. Hence, it is an important consideration from the viewpoint of the erosion rate, which increases the sediment size and quantity of sediment particles in monsoon seasons. (Goodwin et al., 1969).

Several approaches have been employed to mitigate silt erosion and reduce damage in hydropower plants. The primary method involves deploying active sediment chambers to prevent silt particles, typically larger than 0.3 mm, from entering the power plant, thereby facilitating effective de-slitting of suspended particles. Additionally, real-time water monitoring aids in comprehending silt concentration, size distribution, mineral composition, and other factors, serving as an early warning system for hydropower facility operations. While complete elimination of sediments is impractical, efforts must be made to reduce them to a level that maintains the stream carrying capacity and prevents turbine and components from wear (Bishwakarma & Støle, 2008; Singh & Kumar, 2016; Rai & Kumar, 2017). Another approach involves using high-strength blade materials and preventative surface coatings for high-velocity applications, acting as a barrier between the turbine material and the working environment. The effectiveness of various surface engineering processes such as high velocity oxygen-fuel thermal coating processes, friction stir processes, and so on was presented by Prashar et

al. (2020), to counteract slurry erosion failure in hydrodynamic turbines. In the study, factors such as impingement angle, erodent size and shape, slurry concentration, and coating process are crucial considerations in this strategy.

However, introducing the injection of a secondary fluid onto turbine component surfaces is a novel approach to mitigate the impact of silt particles. While secondary fluid injection is traditionally associated with cooling actions in gas turbines and air injection is also used to improve the dissolved oxygen of water facilities (Bunea et al., 2014), but the idea of using air injection to reduce the silt erosion has hardly been hitherto explored. In this regard, the closest study was that of Arndt & Ellis (1993) who tested the effect of the air injection in mitigating cavitation erosion and found it very promising in minimizing cavitation erosion with the application of a specially designed hydrofoil of the NACA 0015 profile with air injection holes at the leading edge. Also, Dhiman et al. (2024) have highlighted the importance of air injection in case of guide vanes to fight silt erosion in hydro turbines and exhibited different operating conditions of guide vanes implicating the real time scenarios of hydro power plants. Later, Dhiman et al. (2024) conducted early experiments to demonstrate the approach of air injection in an experimental setup for guiding vanes in hydro turbines. They suggested a reduction of about 27% and 38% in sediment erosion after introducing an air envelope over the surface of different fabricated samples. Guide vane samples and experimental setup both are specially designed for air provisions that allow the envelope of air over the surface of guide vane samples that act as a mitigation medium to increase the life of hydro turbines. The present study thus explores the potential of silt erosion mitigation using air injection in the context of silt erosion in hydro turbines. By examining the multi-phase interaction between particle-water suspension and injected air along the high-pressure side surface of guide vanes, theoretical models are developed to establish erosion equations based on the physics of particle rebound mechanics. Considerations such as angle of attack and particle velocity during interaction are paramount in evaluating the efficacy of this approach.

2. MATHEMATICAL MODEL AND NUMERICAL METHODS

The computational modelling of an aerated hydrofoil positioned within a sand water slurry flow stream involves complex turbulent interactions between distinct fluids and the solid particles. This physical hydrodynamic scenario is described using a three-way coupling of fluid-fluid, solid-solid, and fluid-solid interactions together. The dynamic exchange of momentum between water, air, and silt particles, which represent the primary, secondary, and discrete phases in the system, is then resolved to predict the spatial erosion behavior over streamlined hydrofoil.

2.1. Discrete Particle Model

For slurry flows, the interaction between silt particles (the discrete phase) and water (the continuous phase) is primarily resolved by a coupled Eulerian-Lagrangian framework. Here, the Lagrangian coordinates are responsible for recording the time-averaged particle trajectory by integrating the translation and rotational motion of particles. In such a case, a few considerations are made for simplification, as follows: (1) spherical particles are used; (2) suspended particles are independent of each other, (3) Particle splitting is restricted; (4) particle rotation is neglected and (5) pitting on the hydrofoil is neglected. Hence, they all contribute towards achieving perfect wall collision sites for the particles (Singh et al., 2019), and their motion is governed by Newton's kinetic equation (Grant & Tabakoff, 1975; Li et al., 2019), as shown in equation 1.

The motion of particles is expressed as:

$$m_{\mathrm{p}}\,(d\,\overrightarrow{U_{\mathrm{p}}}/dt) = \sum \vec{F}_{\mathrm{a}} + \vec{F}_{\mathrm{b}} + \vec{F}_{\mathrm{d}} + \vec{F}_{\mathrm{p}} \tag{1}$$

where $\vec{F}_{\mathrm{a}}$, $\vec{F}_{\mathrm{b}}$, $\vec{F}_{\mathrm{d}}$, $\vec{F}_{\mathrm{p}}$ define the forces corresponding to added mass, buoyancy, resultant drag and pressure gradient. Each of these terms can be independently expressed as follows:

$$\vec{F}_a = -\,1/12\,(\pi\, d_p^3\, \rho_p\, d\,\overrightarrow{U_p}/dt \tag{2}$$

$$\vec{F}_b = 1/6\,\pi\, d_p^3\,(\rho_p - \rho)\, g \tag{3}$$

$$\vec{F}_p = 1/4\,\pi\, d_p^3\ \nabla P \tag{4}$$

Where m_{p}, d_{p}, ρ_{p}, U_{p}, and ρ represents the particle mass, particle diameter, particle density, particle velocity, and fluid density. Energy possessed by particles changes continuously under the influence of external body forces, i.e., drag and lift forces followed by rebound against the hydrofoil wall, which in turn manipulates the behavior of carrier fluid. As a result, fluid loses its mean momentum, and turbulence is produced pragmatically due to drag, as recommended by the authors (Zhang et al., 2007; Mansouri et al., 2015; Vieira et al., 2016). The aggregate viscous drag forces acting on a blunt particle are an amalgam of both pressure and skin friction drag, as shown in Equation 5.

Drag force on a silt particle is given as:

$$F_{\mathrm{d}} = \tfrac{1}{2}\,\rho_{\mathrm{g}}\,U^2\,C_{\mathrm{d}}\,A \tag{5}$$

[$A = (\pi/4)\,D^2$, for spherical particle]

Here C_{d} (coefficient of drag) is usually a function of particles geometrical attributes, and while authors Klajbár and Könözsy (2016); Lote et al. (2018) have suggested multiple drag laws, the one established by Morsi and Alexander (1972) is used for spherical particles in this study, which states:

$$C_{\mathrm{d}} = P_1 + (P_2/Re_{\mathrm{f}}) + (P_3/Re_{\mathrm{f}}),\ [R_e = (\rho\ d_{\mathrm{p}}\ |U_{\mathrm{p}} - \mathrm{U}|)\ /\ \mu] \tag{6}$$

Equation 6 includes P_1, P_2, and P_3 constants that are functions of the Reynolds number Re_{f}, where the subscript

Table 1 Values of different constants at a varying range of Reynolds numbers

Re **Range**	**Constants**		
	P_1	P_2	P_3
$0 < Re < 0.1$	0	24	0
$0.1 < Re < 1$	3.69	22.73	0.09
$1 < Re < 10$	1.222	29.16	3.88
$10 < Re < 100$	0.61	46.5	-116.67
$100 < Re < 1000$	0.36	98.33	-2778
$1000 < Re < 5000$	0.357	148.62	-47500
$5000 < Re < 10000$	0.461	-490.546	578700
$Re > 10000$	0.519	-1662.5	5416700

'*f*' denotes the fluctuations between discrete and continuous phases due to the inertial effects. Table 1 provides experimental insight into the variation of these constants as they increase Re_f (Karunarathne & Tokheim, 2017). All the above equations describe the particle trajectories in the prescribed domain under an established flow field. It is necessary to highlight the fact that the location and magnitude of erosion are very sensitive to particle dynamics and pit growth during an impact, which is a stochastic process and requires some sort of statistical explanation. In this study, a state of equilibrium is investigated for appropriate prediction of locations prone to pitting, followed by comparing the effect of aeration under similar circumstances.

2.2. Fluid Flow Model

The solution for the flow field of a fluid is mathematically expressed using incompressible Navier-Stokes equations, which comprise continuity and momentum equations in partial form as defined in Equations 1 and 2.

$$\nabla.\rho\vec{V} = 0, \ [\rho = 0] \tag{7}$$

$$\rho\,(D\,\vec{V}/Dt) = -\nabla.p + \rho.\,\vec{g} + \mu\nabla^2\vec{V} + \vec{S}_m, \ [\rho\,(\partial V/\partial t + (\nabla.\vec{V})\,V] \tag{8}$$

Where ρ, V, p, ρg, and S_M denote the fluid density, instantaneous velocity, pressure, body forces, and change in momentum due to the solid phase, respectively. For multiphase flows involving discrete particles, volume-averaged approximation is done for each phase, and alternate continuity and momentum equations [9, 10] are proposed as follows:

Continuity Equation:

$$\partial/\partial t\,(a_p\rho_p) + \nabla.\,(a_f\rho_f\,V_f) = 0 \tag{9}$$

Momentum Equation:

$$\partial/\partial t\,(a_f\rho_f V_f) + \nabla.\,(a_f\rho_f\,V_fV_f) = -\,a_f\,\nabla P + K_{pf}\,(V_p - V_f) + a_p\rho_p g + \nabla.\,\bar{\bar{\tau}}_f + C_{vm}a_f\rho_f\,(V_p.\nabla V_p - V_f.\nabla V_f) + C_L a_p\rho_f\,(V_f. - V_p)$$

$$\partial/\partial t\,(a_p\rho_pV_p) + \nabla.\,(a_p\rho_p\,V_pV_p) = -\,a_p\,\nabla P + K_{pf}\,(V_f - V_p) + a_p\rho_p g + \nabla.\,\bar{\bar{\tau}}_p + C_{vm}a_p\rho_f\,(V_f.\nabla V_f - V_p.\nabla V_p) + C_L a_p\rho_f\,(V_p. - V_f) \tag{10}$$

Where a_f, ρ_f, V_f and a_p, ρ_p, V_p are the concentration, density, and velocity parameters for fluid and solid particles, respectively. $\bar{\bar{\tau}}_n$is the stress tensor that can be expressed in generalized form as (Zolfagharnasab et al., 2021):

$$\bar{\bar{\tau}}_n = \mu\,[(\nabla.v + \nabla.v^T) - 0.66(\nabla.v.I) \tag{11}$$

Where μ, I represent the molecular viscosity and unit tensor.

Further, ∇P, K_{pf}, C_{vm}, and C_L are responsible for the determination of the static pressure gradient, inter-phase drag coefficient, effective mass-force coefficient, and lift coefficient. The right-hand terms in the momentum equation are the source of uncertainties and should be validated on a case-by-case basis during approximations.

2.3. Multiphase Fluid-Fluid Model

The Eulerian approach facilitates the interaction between water and air after the numerical solution is initiated in order to stabilize the resultant flow field. The relationship between *Re* and C_d is expected to be non-linear beyond $Re > 1$ or when the particles are above the Kolmogorov scale (Kaufmann, 2004). Hence, an appropriate selection of drag and turbulence models determines the accurate resolution of the desired flow constituents. In this study, the Schiller-Naumann dynamic drag model is used to satisfy momentum exchange between fluid-fluid mixtures. Silva et al. (2015) previously carried out a similar type of work and reported better agreement with the Schiller – Neumann model than the Gidaspow model.

Momentum exchange coefficient under the influence of drag can be written as (Acharya et al., 2019):

$$K_{fq} = (18\,a_f\rho_f\,a_q\mu_q\,f)/\,\rho_f d_p^2 \tag{12}$$

The subscripts '*f*' and '*q*' in Equation 12 denote the primary phase (water) and secondary phase (air). Drag Function *f* can then be equated as $C_d.Re/\,24$.

C_d can be further calculated by Schiller-Naumaan expression:

$$C_d = 24\,(1 + 0.15\,Re_f^{0.687})\ /Re_f : \{\text{when } Re_f \le 1000\}$$

$$C_d = 0.44: \{\text{when } Re_f > 1000\} \tag{13}$$

The author provided relevant experimental evidence (Peng & Cao, 2016), stating that C_d is approximated as 0.445 for a Newtonian fluid mixture within the range of $800 < Re < 3 \times 10^5$. Moreover, it is also deduced from the graphical comparison between several drag models that Morsi Alexander models were in great agreement with the results of the Schiller – Naumann model.

2.4. Turbulence Model

Turbulence is generally modelled by transforming the governing N-S equations into RANS (Reynolds Averaged

Navier-Stokes) form, where the velocity (U_j) is decomposed into its mean ($\overline{U_j}$) and fluctuating (u_j) components (Johansson, 2012). A robust two equation *K-ω* SST (viscous) model is employed for current work, which is a hybrid blend between Wilcox *K- ω* and *K-ℰ* models.

The hybrid nature facilitates the use of the omega model in resolving the boundary layer near the object wall, where the viscous effects are predominant. Also, the adequate wall treatment makes it less sensitive to near-wall effects when compared with the *K-ℰ* model. It is then followed by a smooth transition to the Epsilon model as the flow approaches free stream velocity (U_∞). Moreover, existing literature (Ducoin & Young, 2013; Devolder et al., 2017) provides evidence of higher solution accuracy for problems pertaining to drag estimation, cavitation, hydrodynamic waves, and intermediate-to-high Reynolds flow separation using the SST (Shear Stress Transport) model.

2.5. Erosion Model

A wide array of erosion models has been assembled based on different experimental conditions, typically comprising the Finnie erosion model (Finnie, 1960), Oka erosion model (Oka et al., 2005), McLaury erosion model (McLaury et al., 1995), Grant and Tabakoff erosion model (Grant & Tabakoff, 1975), Ahlert erosion model and Forder erosion model (Forder et al., 1998). A detailed survey of existing literature can be referred by using the author's previous work (Padhy & Saini, 2008; Arabnejad et al., 2015). All of the stated models in general evaluate the erosion rate (ER), which is a function of V_p, θ_p, D_p, Fs_p, BH_t, *and* ρ_t is defined as, particle velocity, particle impact angle, particle diameter, particle shape and size factor, hardness, and density of the target body. The standard expression relating velocity (V^n) and the dimensionless function of impact angle (γ) is proposed in this form:

$$ER = K\,V^n\,f(\gamma) \tag{14}$$

The rebound behavior is then resolved by calculating the normal and tangential coefficients of restitution. The coefficient of restitution is defined as the ratio of the particle's rebound velocity to the impact velocity that accounts for the loss in the particle's kinetic energy after impact. Accurate prediction of particle trajectories is solely responsible for the estimation of erosion rate, and a great deal of studies subjected to hydro abrasive wear have employed the Grant and Tabakoff model in recent times (Acharya et al., 2019; Neopane et al., 2012; Rakibuzzaman et al., 2019). One of the main reasons suggested for the selection is the possibility of modifying a large number of dependent coefficients. However, both the Finnie and Tabakoff models support the fact that the tangential velocity component is the most significant contributor to ductile erosion when compared with the normal velocity component. In this study, simplified model schemes by Finnie and Mclaury were investigated as follows:

2.5.1. Finnie Erosion Model

$$f(\gamma) = 1/3.\ Cos^2\ (\gamma) \text{ if } tan\ (\gamma) > 1/3 \tag{15}$$

$$f(\gamma) = Sin\ (2\gamma) - 3.\ Sin^2\ (\gamma) \text{ if } tan\ (\gamma) \leq 1/3 \tag{16}$$

where values of velocity exponent 'n' for ductile material and model constant 'K' are taken as 3 and 2.12 e-07, respectively, along with a maximum erosion angle 'γ' of 30 degrees for quartz particles (Rakibuzzaman et al., 2019).

2.5.2. McLaury Model

$$K = F\,BH^K \tag{17}$$

$$f(\gamma) = b\gamma^2 + c\gamma \text{ if } \gamma \leq \gamma_{lim} \tag{18}$$

$$f(\gamma) = x.\ Cos^2\ (\gamma).\ sin(w\gamma) + y.\ Sin^2\ (\gamma) + z \text{ if } \gamma > \gamma_{lim} \tag{19}$$

where values of imperial constant (F), Brinell's hardness number (Bh) of the target body, and wall material coefficient (k) are taken as 1.99 e-07, 187, and -0.59, respectively, corresponding to carbon steel. Other model constants *b, c, w, x,* and *y* used for impact angles are taken as -13.3, 7.85, 1, 1.09, and 0.125, respectively. The velocity exponent (n) and transition angle (γ) are kept constant at 3 and 30 degrees.

3. COMPUTATIONAL DOMAIN AND BOUNDARY CONDITIONS

The geometrical details of the physical model used for simulations focused on erosion prediction of hydrofoil under silt laden fluid flow is shown in Fig. 2. The test domain dimensions are 1.76 m in length (stream-wise direction: Y-axis), 0.12 m in breadth (span-wise direction: X-axis), and 1.06 m in height (stream-normal direction: Z-axis) respectively. The incoming fluid passage is then subdivided into primary and secondary inlets to achieve better control by having concentrated injection of particles in the path of hydrofoil itself. Silt particles are only released from the primary region, which has a total area of 0.052 m^2, whereas free stream water enters at a velocity (U_∞) of 10 m/s through all regions with turbulence intensity lower than a value of 0.05%. Also, Zhang et al. (2007) have previously suggested that the erosion estimation becomes independent of the particle concentration above a certain limit, which was later proved by Vieira et al. (2016) in their numerical study on internal pipe erosion. Similarly, Mansouri et al. (2015) performed an impingement jet study with 50,000 particles for gas-solid and liquid-solid cases to conclude that erosion results were independent of the particle count. The statistical analogy stands true for the present study, and hence 12,900 incoming particles per cycle are similarly found adequate, where one cycle corresponds to ten iterations. This is achieved using the Rosin-Ramler method, where a discrete cycle of injections for a range of particles accounts for 100% mass fraction for each size interval. Here, the minimum size of 0.08 mm, maximum size of 0.2 mm, and average size of 0.1 mm particles are selected as input constraints to closely match the sieve test data that was experimentally determined by collected sediment samples from three different hydropower plant sites and around 1 kg of these sample each

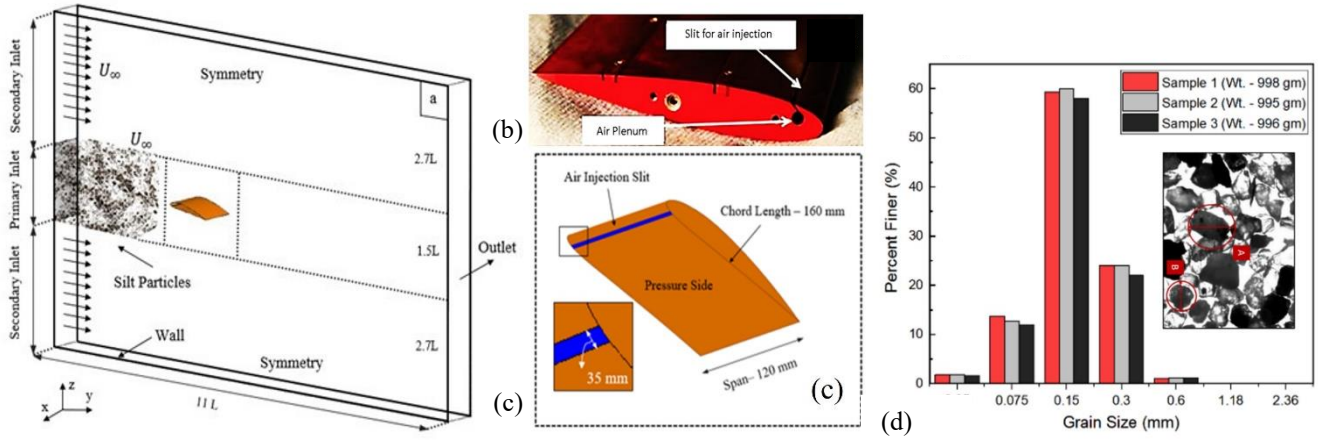

Fig. 2 Geometrical details of physical model used in simulation shown in (a), (b) and (c)

shows different grain size. Most of the sediment particles fall under a range of 0.15 mm of grain size. (as shown in Fig. 2 (d)).

The resultant slurry flow then strikes the hydrofoil obstruction, which is taken as a NACA 4412 profile having a chord length ($y = L$) of 0.16 m and a span equal to the aforementioned domain breadth, which is the baseline case. Reynolds number (Re_L) of 1.22 e10^6 against L at various angles of attack is responsible for the boundary layer thickness, where Reynolds number is defined by ($Re_y = \rho U_\infty y / \mu$) and ρ, μ are the density and kinematic viscosity of water. Further, to evaluate the erosion characteristics under aeration, a source of air injection at distance ($y = 8/L$) from the leading edge is provided as a continuous slit with an aspect ratio (L_x / L_y) of $AR = 3.52$, which is referred to as the aeration case. This particular anatomy for injection is selected in order to satisfy the Coanda effect and consequently allow air to form a shielding blanket on the pressure side of the blade. It is expected to mitigate the trajectories of particles spatially and reduce the overall erosion magnitude, which primarily occurs during impact interaction impact. However, it is also important to consider the drag (C_d) variation arising in such a case and identify suitable tradeoff strategies at different exit velocities(U_a) of air. 'No-slip' condition is only valid near hydrofoil wall, whereas the viscous-shear effect ($\tau = \mu\ (\partial u/\partial y)$) is neglected on other remaining walls within the domain by using periodic symmetry for side walls and specifying (shear stress = 0) for top and bottom walls, respectively. This is done to idealize an actual sea-stream condition and avoid any particle reflection against the wall that might make the case sensitive to unreasonable particle interactions and provide misleading arguments. Domain outlet is employed at zero-gauge pressure, which represents *(∂w∂x =∂w∂x =∂w∂x = 0)*. Any effect of temperature variation is not considered in this study, and the boundary conditions are subjected to a 30° C ambient temperature.

The present study has employed commercial software package Fluent 19.1 to carry out coupled interaction between primary phase refers to the main fluid phase in the system which is water, secondary phase refers to another fluid phase present in the system which is air or bubble dispersed within the primary phase , and discrete phase refers to individual particles or entities that are distinct from the continuous fluid phases such as silt particles, by integrating the viscous model *K*-omega SST, this type of turbulence model used to simulate the effects of fluid viscosity and turbulence on flow behavior; with the Multi-phase model that allow to simulate the behavior of multiple fluid phases within a single computational domain and the discrete phase model to simulate the motion and behavior of individual particles or droplets within a fluid flow. It tracks the trajectories of discrete particles based on forces acting on them.

A pressure-based solver is used to resolve the governing equations over control volumes for achieving the steady-state solution. An expensive coupled algorithm that simultaneously solves for all variables with pressure interpolation is preferred over simple formulations to control accuracy and establish an accelerated convergence error limit set at 1 e-06. A second-order upwind scheme is used to discretize the non-linear convective terms within momentum equations, followed by the viscous terms.

4. NUMERICAL VALIDATION

The accuracy of the numerical method is validated by examining the grid sensitivity (Sadrehaghighi et al., 1992; Bogey, 2018; Koomullil et al., 2008). For this purpose, Cartesian cut-cell and O-grid hexa methods are utilized in devising high-order grids for the simulation as illustrated in Fig. 3, Fig. 4, and Table 2. The spherical particles are used under specific assumptions which include the independence of suspended particles from each other, restrictions on particle splitting, neglecting particle rotation,

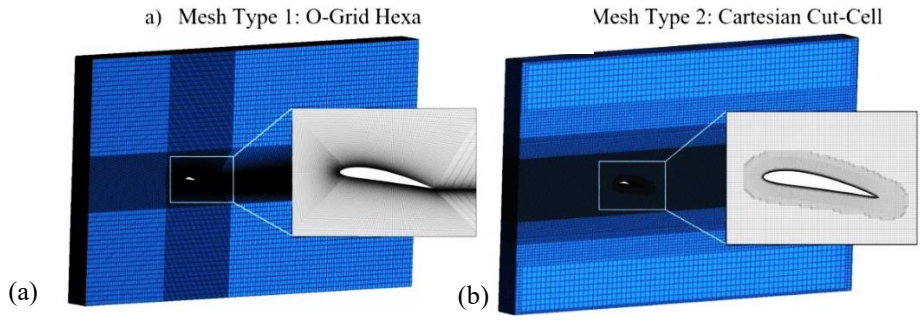

Fig. 3 Details of the computational grid

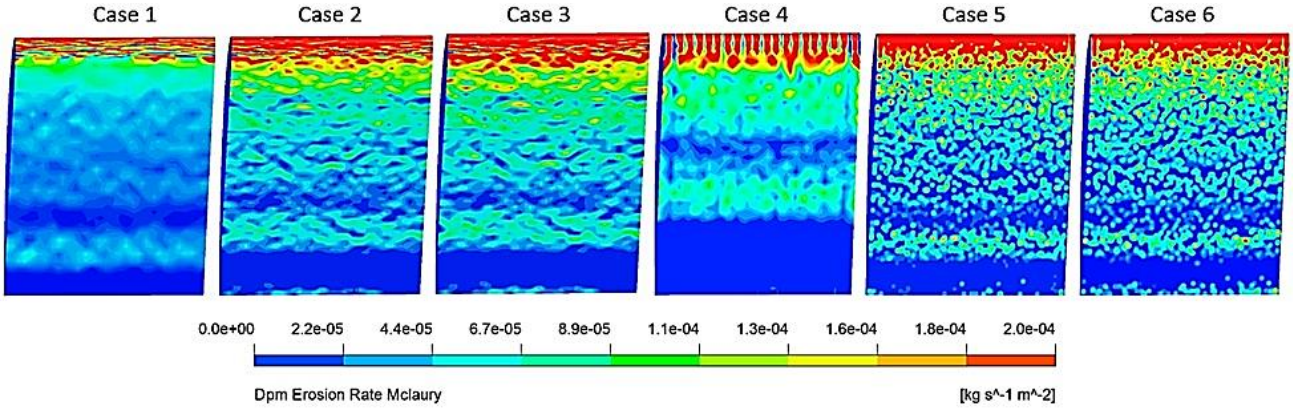

Fig. 4 Grid refinement test results for estimation of erosion behavior on pressure side of hydrofoil using two mesh types: O-grid hexa (Cases 1-3) and Cartesian Cut cell (Cases 4-6)

Table 2 Details of the element count, coefficient of Drag and Erosion rate for different mesh types

Mesh Type	O-Grid Hexa			Cartesian Cut Cell		
	Case-1	Case-2	Case-3	Case-4	Case-5	Case-6
Element Count (million)	0.949	1.276	1.401	0.51	1.04	1.241
Coefficient of Drag (C_d)	0.696	0.674	0.651	0.716	0.648	0.644
Erosion rate (kg/m^{2}s)	1.25 e-03	7.26 e-04	8.84 e-04	1.48 e-04	8.71 e-04	9.11 e-04

and disregarding pitting on the hydrofoil. These assumptions collectively aim to ensure optimal conditions for particle-wall collisions. The velocity of solid particles is determined by Newton's kinetic equation within the Discrete Particle Model and by the particle momentum equation in the Fluid Flow Model. Additionally, the erosion model considers the properties of the wall material, employing a ductile material characterized by a wall material coefficient of k = -0.59. This structured approach ensures a coherent narrative, beginning with the validation of the numerical method and proceeding to detail the simulation setup and underlying conditions.

The appropriate prediction of drag attributed to viscous effects normal to the hydrofoil wall depends on the accuracy of boundary layer resolution, which is directly proportional to the level of refinement. In order to achieve this while using the *K*-omega model for low Reynolds flow, it is preferably required to have a dimensionless distance $y^+ \leq 5$ which refers to the threshold between the viscous sublayer and buffer layer. Here, y^+ is defined (Reichardt, 1951) as: $y^+ = y.u_\tau/\nu$, where y is the first cell height, u_τ is the frictional velocity, and ν is the kinematic viscosity. In the present case, 24 inflation layers with a growth rate of 12% between consequent layers and a bias factor of 36 are selected to maintain y^+ below 5 for both cut-cell and O-grid mesh types, respectively. It is also noteworthy to mention that with increasing angle of attack, the resolving buffer regime ($5 < y^+ < 30$) and logarithmic regime ($y^+ > 30$) are considered insignificant as they fail to provide any reasonable effects.

5. RESULTS AND DISCUSSIONS

The presented study aims to significantly contribute to the longevity of hydro turbines by exploring the novel approach of secondary fluid injection to mitigate silt erosion. However, the study doesn't delve into other operational parameters, keeping ahead the objective of the study.

Nonetheless, the study's value lies in its innovative approach and its potential to enhance turbine life in a productive and resourceful manner without compromising the material properties of the blades and other components.

This study analyzes the erosion effects of silt content, air-water phase interactions, and flow dynamics around a guide vane used in Francis turbines with the NACA 4412 hydrofoil. The O-Grid Hexa mesh element counts are 0.949, 1.276, and 1.401 million for cases 1, 2, and 3, respectively. While the Cartesian Cut mesh counts are 0.51, 1.04, and 1.241 million for cases 4, 5, and 6 respectively, also presented in Table 2. Operational parameters include silt concentration in water stream (m) of 2500 ppm and 5000 ppm, velocity of air injection (v) from 7.5 m/s to 17.5 m/s, the angle of air injection or degree of air injection at which air is injected on the surface (d) of 30° and 90°, angle of attack of the hydrofoil (a) of 10° and 20°, and a free stream velocity of 10 m/s. The Euler-Euler-Lagrange model with the K-omega SST turbulence model predicts erosion wear behavior with and without air injection. Air injection is from a continuous slit at y = 8/L from the leading edge with an aspect ratio (AR) = 3.52. Simulation accuracy is validated using the grid sensitivity method.

5.1. Effect of Air Injection in Mitigating Silt Erosion

Simulations and numerical analysis in the present study has been established that air injection on the surfaces of guide vanes can mitigate silt erosion. The simulated object used is ventilated guide vane similar to the ventilated hydroturbine used in previous study (Arndt & Ellis, 1993). It has been observed from the simulation results that air injection helps mitigate silt erosion in the following ways:

5.1.1. Creating a Buffer Zone

It is believed that air on the surface of the guide vane works as a buffer and creates a cushioning effect that reduces the impact of silt particles on the surface of the vane. This assists in decreasing the abrasive wear generated by the silt particles present in the water stream. Also, by forming a membrane of separation between the water and silt particles, air in the water flow can decrease the shear stress applied to the surface of the blades. This reduces the abrasive impact caused by silt particles in the water stream on the guide vanes.

5.1.2. Modifying the Mechanics of Flow

When air is added, the water's flow characteristics change, delivering the silt particles more uniformly throughout the water stream. From simulation images, it can be observed that this can minimize localized erosion by preventing the accumulation of silt particles on certain surfaces of the turbine components. Furthermore, following air injection, which lowers the effective kinetic energy of the water stream, the apparent density of the water is also decreased. Consequently, the influence of silt particles on the surfaces has diminished, thereby diminishing the intensity of silt erosion.

5.1.3. The Carrying-Away Effect

From the results, it has been seen that the air injected helps in carrying away parts of the silt particles in the water stream, avoiding accumulation and impact at one place on the vane surface. This continual draining activity can help keep the surfaces of the guide vane cleaner while lowering the possibility of silt erosion. This effect is dependent on the velocity of the air injection and the angle of the air injection, as these two parameters mark the impact on the carrying-away effect, which really plays a major part in mitigating the silt erosion.

5.2. Simulation Results with and Without Air Injection

The simulation findings pertaining to air injection demonstrate a significant decrease in the erosion rate. Based on the information presented in Fig. 5, it is apparent that by maintaining constant values for variables a and m and introducing air at d=30° with a v=7.5 m/s, the reduction in erosion is of around 56%. This analysis disregards the initial impact caused by silt-laden water. A common observation in both scenarios is that upon first contact with the surface, water induces a significant erosion rate. However, this rate subsequently diminishes down the profile. Further, it seems that the erosion rate is very consistent in both scenarios and remains at a low level. This is due to the particle separation from the profile surface, which limits the silt-laden water from affecting the surface of the profile.

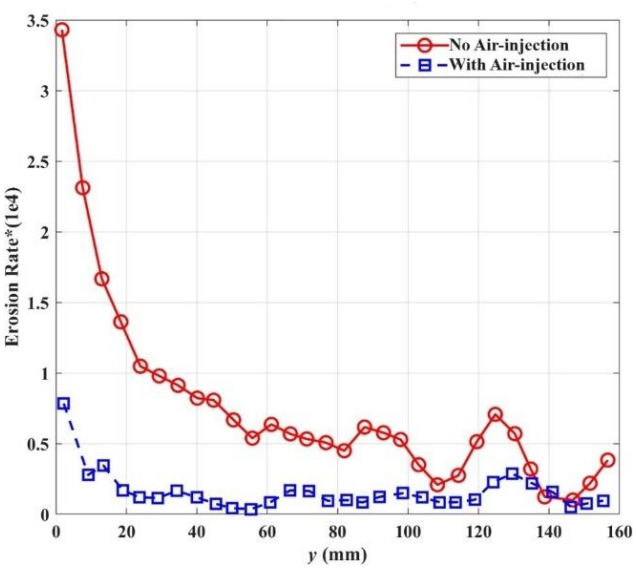

Fig. 5 Erosion rate vs span of guide vane without and with air injection for a=10°, m-2500 ppm, d=30° and v=7.5 m/s

Moving forward, when m=5000 ppm, as shown in Fig. 6, the following comments can be made. First, the pattern of erosion rate with and without air injection is quite similar to the previous case. Second, the erosion rate with and without air injection is considerably higher as compared to Fig. 5. This change is there because of the increase in the value of

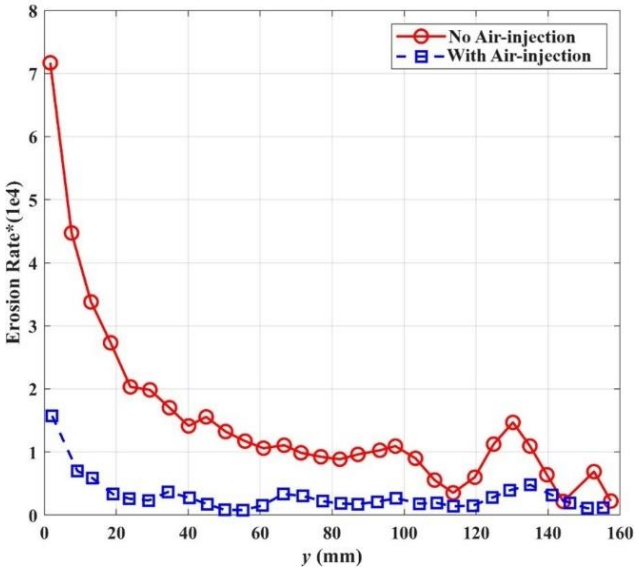

Fig. 6 Erosion rate vs span of guide vane without and with air injection for *a*=10˚, *m*=5000 ppm, *d*=30° and *v*=7.5 m/s

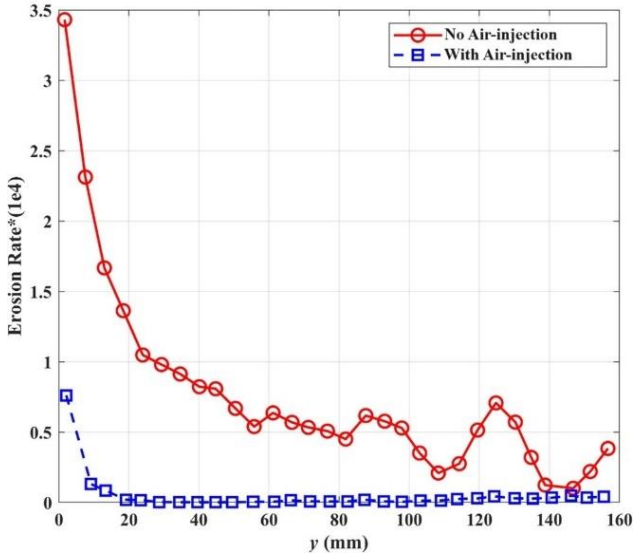

Fig. 7 Erosion rate vs span of guide vane without and with air injection for *a*=10°, *m*=2500 ppm, *d*=30° and *v*=17.5 m/s

m. As *m* increases, the number of silt particles increases, the impact caused by the particles increases, which leads to more wear and erosion on the surface area. But with the introduction of air injection, it can be seen that the erosion rate drops with a considerable amount and leads to less erosion.

Following the change in velocity of air injection from Fig. 7, it can be perceived that with increasing velocity, the value of the erosion rate drops significantly, giving a great sense that the erosion rate is about to reach zero. Initially it

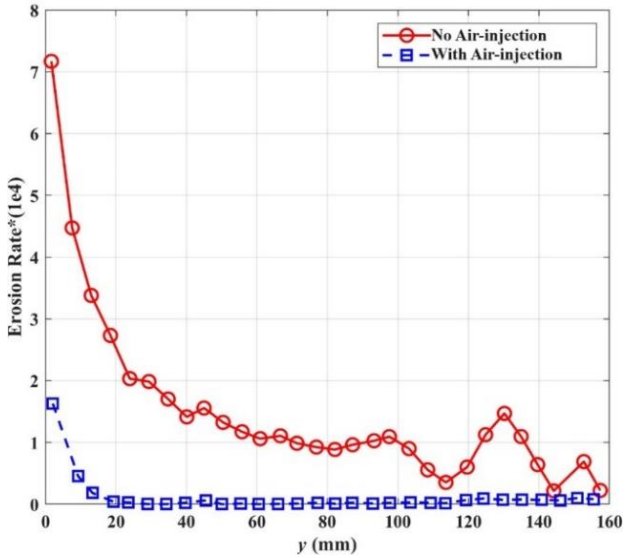

Fig. 8 Erosion rate vs span of guide vane without and with air injection for *a*=10°, *m*=5000 ppm, *d*=30° and *v*=17.5 m/s

has some values greater than one, but later on, the whole span of the vanes seems to be less than one and near zero. Even with no air injection moving further along the span, the erosion rate decreases, but not as much as in the case of air injection. Continuing with this velocity of air injection when the *m*=5000 ppm, there is a substantial increase in the value of silt erosion in the case of no air injection, but if we look at the blue line in Fig. 8, it seems the same as in the previous case, meaning a very low erosion rate. It seems that even with the increase in the values of *m*, air injection is playing its role very adroitly and allowing the silt erosion rate to be as minimal as it can be, which is near zero. When *m* increases, it seems that the erosion rate increases. This is obvious because as the number of particles increases, silt-laden water has a greater tendency to wear the surface of guide vanes. However, as we can see from Fig. 6 and Fig. 8, *m* is increased and with the help of air injection, we can still see a notable difference in the erosion rate, which ultimately increases the life span of the components of the hydro-turbines. The most significant observation from Fig. 5 to Fig. 8 is that the line representing the erosion rate exhibits minimal vertical displacement from the reference point and remains mostly horizontal near the x-axis. This indicates that the silt erosion rate can be significantly reduced, approaching zero, through the implementation of the air injection technique. Consequently, it can be suggested that the utilization of this technique has the potential to enhance the operational life of turbine blades and other turbine components.

Further moving forward, we have compared different parameters through the simulation within the air injection and tried to find optimized values for injecting air to mitigate silt erosion. However, every case has consistently shown

that there is a decrease in silt erosion compared to the cases without air injection.

5.3. Effect of Velocity of Air Injection

The *v* is an essential factor that can substantially affect the performance of the air injection concept in mitigating silt erosion. It appears from the results that higher velocities keep the silt particles elevating and suspending in the water stream, which allows them not to strike to the surfaces and minimizes the risk of silt erosion in hydroturbines. The localized patterns of flow surrounding the guide vanes can be altered when air injection velocity is increased. This has an impact on the paths and likelihood of sediment particle impingement on turbine surfaces. Also, at higher velocities, the dissemination of air bubbles is proper, which allows air to create a more efficient layer over the surface, which minimizes the direct contact between the surface and the silt particles in the water stream.

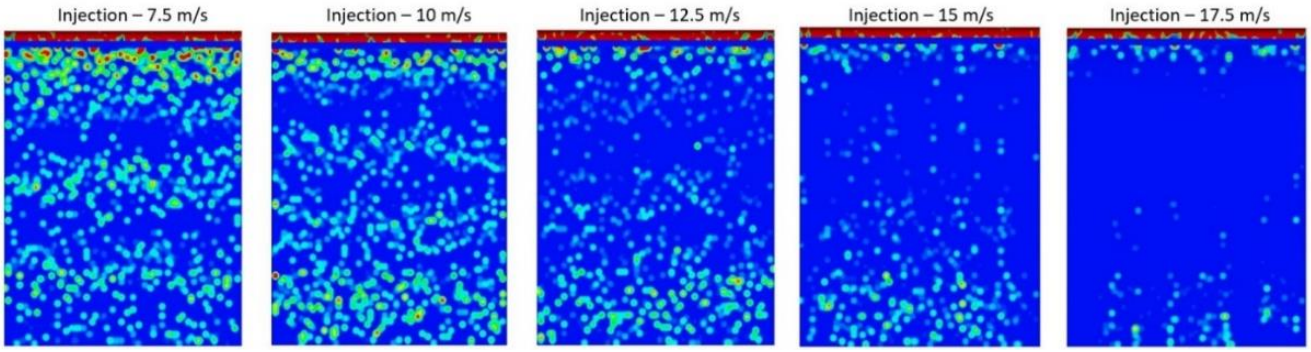

Fig. 9 Simulation showing images for different velocities of air injection for *a*=10°, *m*=2500 ppm and d=30°

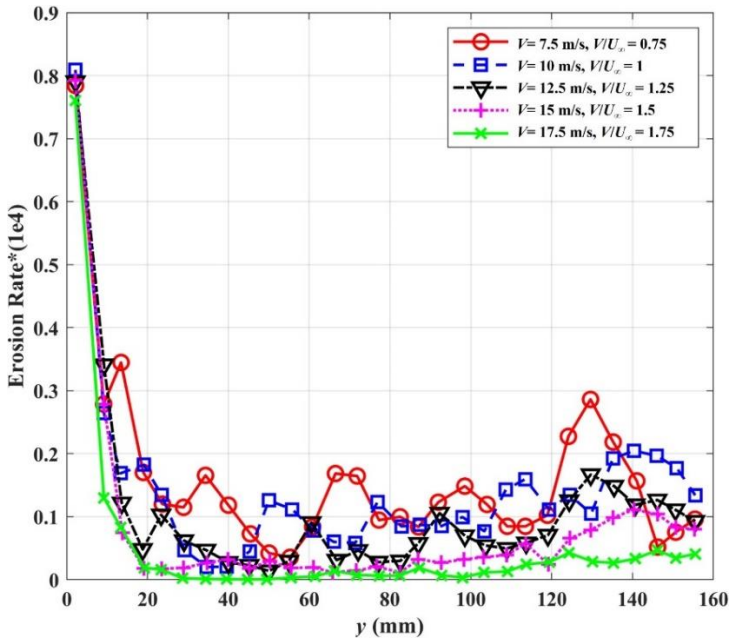

Fig. 10 Erosion rate vs span of guide vane with different velocities of air injection for *a*=10°, m=2500 ppm and *d*=30°

5.3.1. Case-1 (*a*=10°, *m*=2500 ppm and *d*=30°)

From Fig. 9 and Fig. 10, it can be seen that with the increase in the value of *v*, there is a decrease in the rate of erosion; however, initially, every velocity show almost the same value of the erosion rate, but later, moving on the span, higher velocities are showing better results, a reduced rate of silt erosion. In Fig. 9 and Fig. 10, it can be seen that parameters are considered as *a*=10°, *d*=30° and *m*=2500 ppm while varying the values of *v*. All of these cases involve air injection over the span of the guide vane. The green color line (in Fig. 10) shows the best result where the rate of erosion is nearly zero or less than 0.1 for most of the span. Therefore, it can be stated that a guide vane running under this condition will have more life as compared to all the other cases.

5.3.2. Case-2 (*a*=10°, *m*=2500 and *d*=90°)

In the following case, the value of *d* is changed from 30° to 90°, and the changes we have seen in the simulation images are shown in Fig. 11 and Fig. 12. The changes in the rate of erosion with varying *v* are almost the

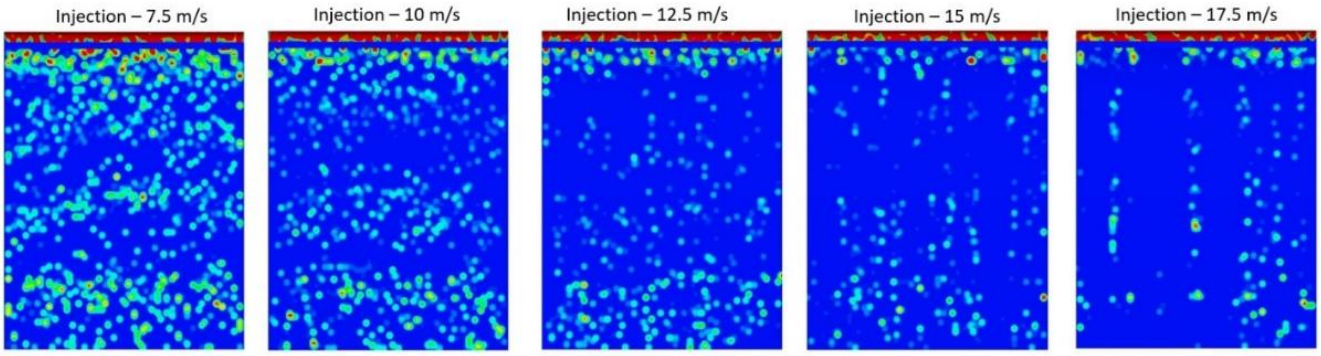

Fig. 11 Simulation showing images for different velocities of air injection for *a*=10°, *m*=2500 ppm, and *d*=90°

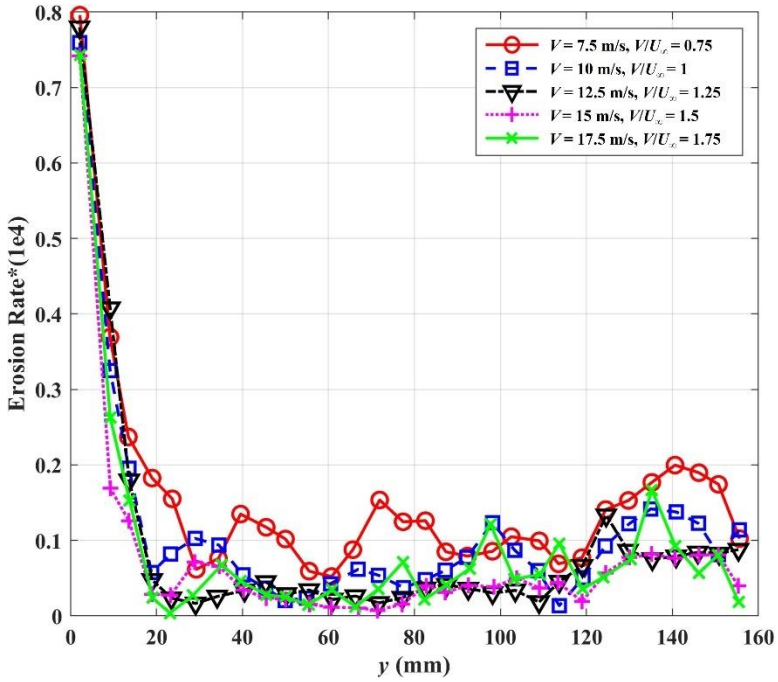

Fig. 12 Erosion rate vs span of guide vane with different velocities of air injection for *a*=10°, *m*=2500 ppm and *d*=90°

same as they were in the earlier case, except for case 5, when *v*=17.5 m/s, where in the last case it was the minimum rate of erosion, whereas here it is not. In this case, the minimum erosion rate can be seen when *v*=12 m/s. However, comparing Fig. 9 and Fig. 11, it can be observed that silt particles are more homogeneously mixed in the case when *d* is increased and they are farther away from the surface of the guide vane. Not only that, but from Fig. 10 and Fig. 12, it can be seen that, until case 4, the effective rate of erosion is at its minimum when *d*=90°.

Air injection on hydro turbines is a highly complex and intricate phenomenon; thereby, answering for any change in the system will be a combination of multiple things. For the sake of subject matter, it can be inferred that by increasing *d*, the envelope made by air bubbles has some more room to cover and is providing a better buffer for the layer of air. This allows silt particles to hardly make any contact with the silt particles. However, as earlier said and shown, air injection is a convoluted phenomenon. In other cases, we can see which there are alterations in the values of the rate of erosion at higher *v* and *d*. in *v*, but if *d* is increased, we can see some better results until we increase the velocity to 17.5 m/s. Here, the higher *v* and *d* have changed the whole characteristics of water flow and mixing behavior over the surface of the guide vane, due to

5.3.3. Case-3 (*a*=10°, *m*=5000 ppm and *d*=30°)

Moving ahead, *m* is changed from 2500 ppm to 5000 ppm. Simulation results on the span of the guide vane are shown in Fig. 13, and the rate of silt erosion with changes in *v* is shown in Fig. 14. Contrasting Fig. 9 and Fig. 13, it can be confirmed that figures show that the amount of silt particles is increased in the water stream due to which the amount of silt erosion has definitely increased, but as we

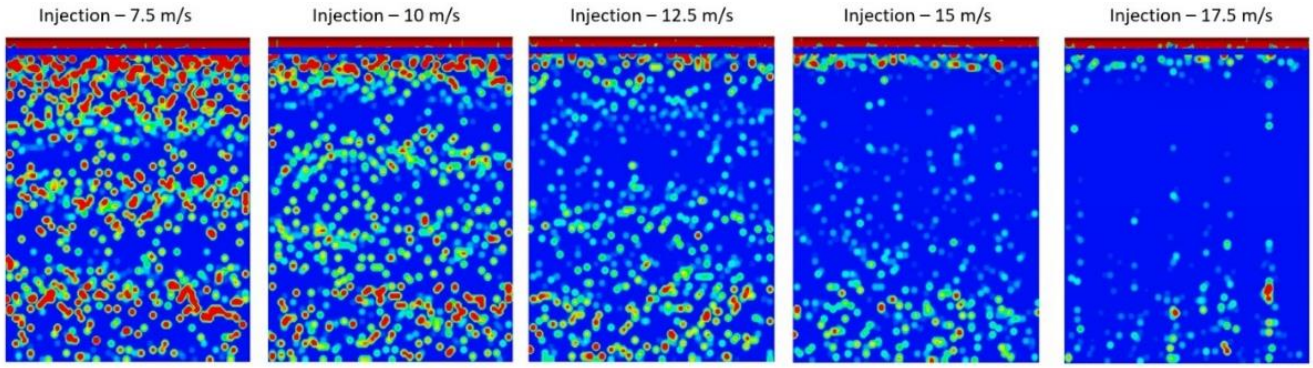

Fig. 13 Simulation showing images for different velocities of air injection for *a*=10°, *m*=5000 ppm and *d*=30°

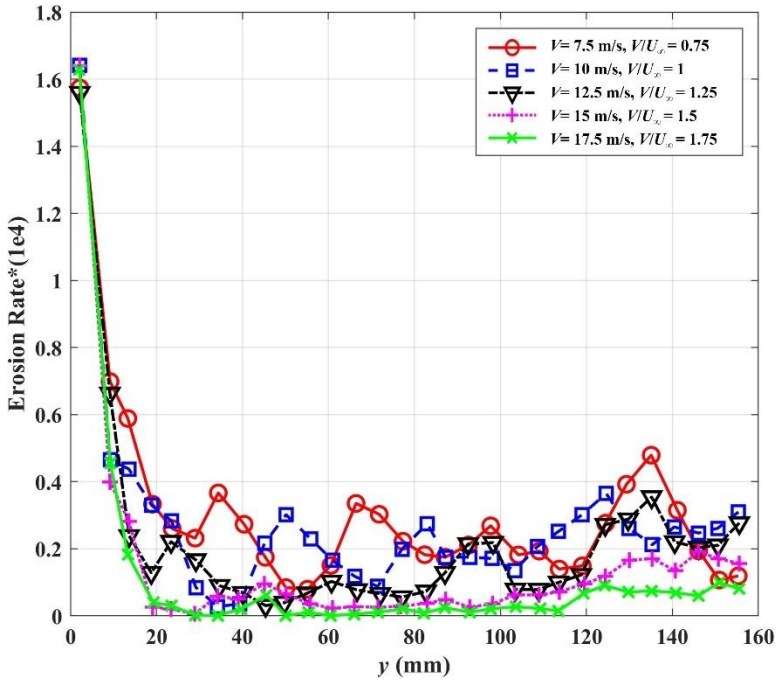

Fig. 14 Erosion rate vs span of guide vane with different velocities of air injection for *a*=10°, *m*=5000 ppm and *d*=30°

have already established, it is still less than no air injection condition. From the figures, it can also be confirmed that increasing *v* has a positive effect, allowing the silt erosion rate to be minimal.

However, comparing Fig. 10 and Fig. 14, we can interpret that yes, there is an increase in the rate of erosion when the silt particles are increased, yet with the introduction of air injection, it can be dragged down to the horizontal axis that is near zero, and with the increase values of *v*, the line is nearly touching the horizontal axis, proving the phenomenon to be very fruitful and practical for the mitigation of silt erosion in hydro-turbines.

5.3.4. Case-4 (*a*=10°, *m*=5000 ppm and *d*=90°)

Advancing in the comparison of the parameters, now the value of *a*=90° and the *m*=5000 ppm. For this case, there can be multiple comparisons, first and foremost with and without air injection, which results in the conclusion that air injection allows a reduction in the rate of erosion, as can be inferred from Fig. 16. The second comparison is when *m*=2500 ppm and *d*=90°. This comparison can be made with Fig. 12 and Fig. 16, and it can be perceived that as *m* increases silt erosion rate also increases, but still far less than the case of no air injection as shown in Fig. 6. The third comparison can be made between the values of *a* keeping silt concentration constant, and this can be presented with the help of Fig. 14 and Fig. 16. Once again, this outcome is consistent with the discussion in Case 2, in which we confirmed that increasing the value of *d* not only enhances the efficacy of air injection but also gives a whole new pattern to the flow of a water stream consisting of silt particles. Also, Fig. 14 shows the lowest value of erosion rate is at *d*=30° and *v*=17.5 m/s. However, in the case of *d*=90°, it is at *v*=12.5 m/s in Fig. 16.

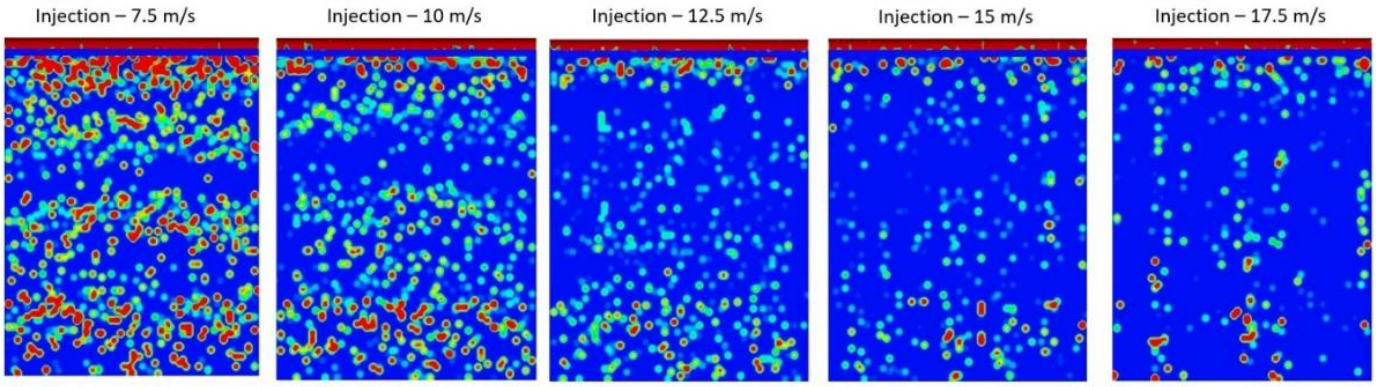

Fig. 15 Simulation showing images for different velocities of air injection for *a*=10°, *m*=5000 ppm and *d*=90°

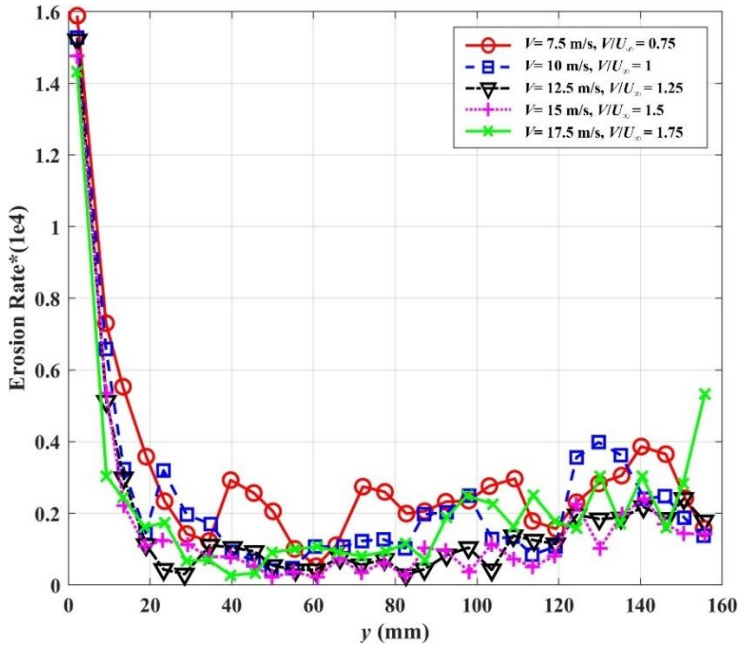

Fig. 16 Erosion rate vs span of guide vane with different velocities of air injection for *a*=10°, m=5000 ppm and *d*=90°

However, if we look closely and compare the cases when we have a higher value of *d*, we can deduce that we have better results and the reduced value of the erosion rate, except for the case when the value of *v* is higher which shows that there is no need to increase *v* for higher values of *d*.

To make some other deductions from the simulation and for further research on the air injection topic, the value of *a* is increased and the simulations for the same velocities but for *d*=90° and keeping *m*=5000 ppm. The results are discussed in Case-5 and the results will show what changes have been observed in making those changes in the profile parameter.

5.3.5. Case-5 (*a*=20°, *m*=50 ppm, and *d*=90°)

When we increase *a*, then a lot is unfolded, which leads to an increase in the lift forces and drag forces acting at the surface of the profile. These forces bring about changes in flow patterns and transform the pressure distribution on the surface of the profile. Although we know that higher *a* value will directly increase the power harnessing capacity but will subsequently increase the values of erosion rates. Thus, the value *a* can be tailored for the hydro-turbines' optimum power and efficiency by achieving a suitable balance between drag and lift forces.

However, simulation results are no different from other cases; the results show that the values of erosion rates are lower than in cases without air injection, but it has been established that the flow dynamics are more turbulent in this case; henceforth, it has become more complex, and thereby, the values of erosion rate are higher than in the case of a lower value of *a*. Fig. **17** shows the impact of silt particles over the span of the guide vane and comparison of different cases. Another reason is that here the value of *m*=5000 ppm,

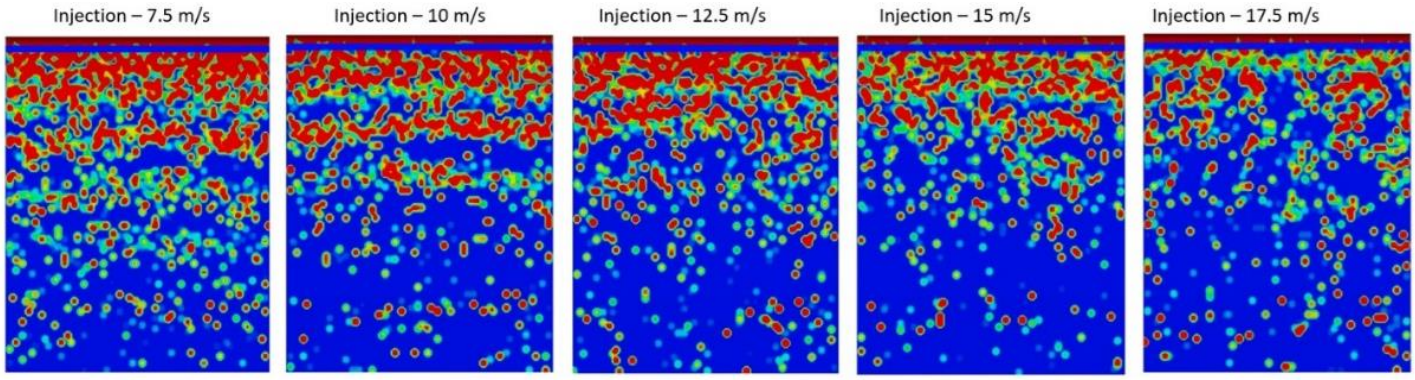

Fig. 17 Simulation showing images for different velocities of air injection for *a*=20°, *m*=5000 ppm and *d*=90°

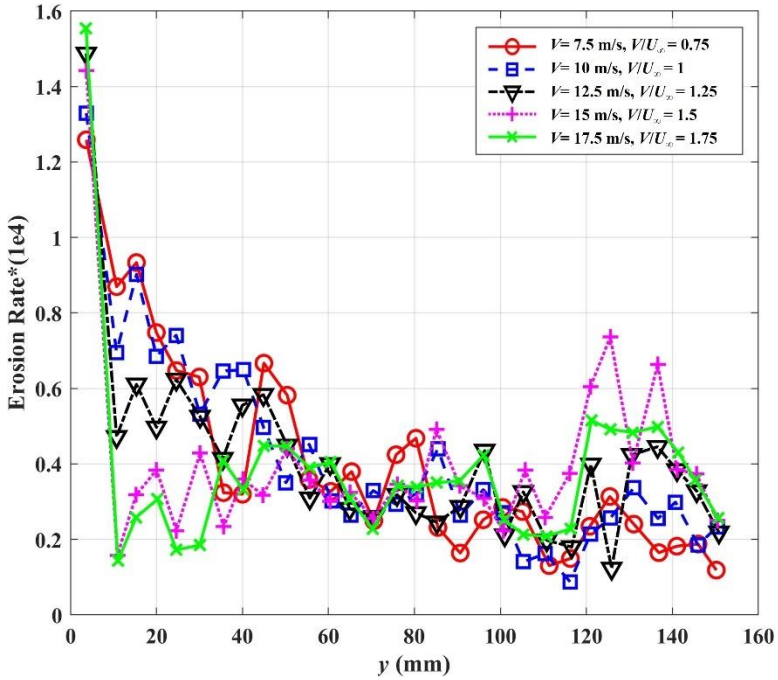

Fig. 18 Erosion rate vs span of guide vane with different velocities of air injection for *a*=20°, *m*=5000 ppm and *d*=90°

in which it is obvious to have more erosion. Higher velocities will lead to making the silt particles separate out the from water stream over the surface of the profile. Fig. ***18*** shows the values of the rate of silt erosion over the span of the guide vane. Although increasing value of *v* is showing better results, providing minimum values of silt erosion rates, the effective patterns of the velocities over the span of the guide vane are more or less the same. As shown in Fig. 18, it can be observed that in the middle of the span, it hardly matters what the velocity is; almost every velocity shows a similar result. It can be observed that the higher value of *a* has increased the turbulence; with higher velocities, it gets more complex. However, air injection is doing its fundamental work of reducing silt erosion, but not better than the lower values of *a*, because of the complexity of the system.

6. Conclusion

In conclusion, the efficacy of air injection on hydro turbine surfaces in mitigating silt erosion is addressed in the present study. Significant advantages have been demonstrated using simulations with varying operating conditions for a NACA 4412 profile of guide vane. The simulation initially compared the cases of erosion rate with and without air injection, which shows the carrying-away nature of air that allows the movement of silt particles from the guide vane, which reduces the risk of damaging the surface. Also, from the simulation, it is established that a shield of air is formed on the surface of guide vane, that reduces the momentum of silt particles and consequently reduces the impact about 66% at *m*=5000 ppm and about 78% at *m*=2500 ppm. Later, in the study, different operating parameters are studied, which concludes that the angle and

velocity of air injection play a vital role. It is observed that for v=7.5 m/s to 17.5 m/s keeping m=2500 ppm, a=10° and d=30°, it produces the maximum reduction of about 70% in erosion rate after the initial impact of silt particles on the guide vane span. When the value of a=90°, the maximum reduction is observed at 12.5 m/s and around 40% reduction in erosion rate.

The study shows promising results, and these findings present a rich simulation datasheet to get a better know-how of the evolving phenomenon of air injection in mitigating silt erosion in hydro turbines. The life of hydro turbines affects the power plant because hydro turbines are the heart and most expensive component of the power plant. Replacing and repairing them requires a lot of energy and expense. Thereby, increasing the life of a hydro turbine will decrease the cost of power production as well as the environmental impact caused by the powerplant by reducing the energy required to run the plant. The implications extended beyond the theoretical insights, impacting practical applications and decision-making in power plant operations. By enhancing the lifespan of hydro turbines, this research contributes to cost reduction in power production and minimizes the environmental footprint associated with hydropower facilities.

ACKNOWLEDGEMENTS

Authors acknowledge the support received from Early Career Research Award, Science and Engineering Research Board, Department of Science and Technology, India under the grant no. ECR/2017/002945, as well as the support received under UPES-SEED grant program from the UPES, Dehradun.

CONFLICT OF INTEREST

The authors declare that they have no known competing financial interests or personal relationships that could have appeared to influence the work reported in this article.

AUTHORS CONTRIBUTION

Prashant Dhiman: Conceptualization, methodology, data collection, formal analysis, writing and editing the original draft. **Ashutosh Bhat:** Conceptualization, methodology, data collection, formal analysis, writing the original draft. **Ashish Karn:** conceptualization, methodology, data collection, supervision, validation, Writing – review and editing, manuscript revision.

REFERENCES

Acharya, N., Trivedi, C., Wahl, N. M., Gautam, S., Chitrakar, S., & Dahlhaug, O. G. (2019). Numerical study of sediment erosion in guide vanes of a high head Francis turbine. *Journal of Physics: Conference Series*, *1266*(1). https://doi.org/10.1088/1742-6596/1266/1/012004

Arabnejad, H., Mansouri, A., Shirazi, S. A., & McLaury, B. S. (2015, September 28). *Evaluation of solid particle erosion equations and models for oil and gas industry applications.* Day 2 Tue, September 29, 2015. https://doi.org/10.2118/174987-MS

Arndt, R. E. A., & Ellis, C. R. (1993). investigation of the use of air injection to mitigate·cavitation erosion.

Bahadur, S., & Badruddin, R. (1990). Erodent particle characterization and the effect of particle size and shape on erosion. *Wear*, *138*(1–2), 189–208. https://doi.org/10.1016/0043-1648(90)90176-B

Bishwakarma, M. B., & Støle, H. (2008). Real-time sediment monitoring in hydropower plants. *Journal of Hydraulic Research, 46*(2), 282–288. https://doi.org/10.1080/00221686.2008.9521862

Bogey, C. (2018). Grid sensitivity of flow field and noise of high-Reynolds-number jets computed by large-eddy simulation. *International Journal of Aeroacoustics*, *17*(4–5), 399–424. https://doi.org/10.1177/1475472X18778287

Bunea, F., Bucur, D. M., Ciocan, G. D., & Dunca, G. (2014). *Aeration solution of water used by hydraulic turbines to respect the environmental policies.* 2014 International Conference and Exposition on Electrical and Power Engineering (EPE), 1015–1020. https://doi.org/10.1109/ICEPE.2014.6970062

Devolder, B., Rauwoens, P., & Troch, P. (2017). Application of a buoyancy-modified k-ω SST turbulence model to simulate wave run-up around a monopile subjected to regular waves using OpenFOAM®. *Coastal Engineering*, *125*, 81–94. https://doi.org/10.1016/j.coastaleng.2017.04.004

Dhiman, P., Bhat, A., & Karn, A. (2022, October). The Efficacy of Air Injection in Mitigating Silt Erosion on Hydroturbine Blades: A Computational Study. In *International Conference on Hydro and Renewable Energy* (pp. 437-444). Singapore: Springer Nature Singapore.

Dhiman, P., Singh, V. P., & Karn, A. (2024). Experimental and computational analysis of air injection as a mitigation technique for silt erosion in hydro turbines. Renewable *Energy and Sustainable Development*, *10*(2), 345. https://doi.org/10.21622/resd.2024.10.

Ducoin, A., & Young, Y. L. (2013). Hydroelastic response and stability of a hydrofoil in viscous flow. *Journal of Fluids and Structures*, *38*, 40–57. https://doi.org/10.1016/j.jfluidstructs.2012.12.011

Finnie, I. (1960). Erosion of surfaces by solid particles. *Wear*, *3*(2), 87–103. https://doi.org/10.1016/0043-1648(60)90055-7

Forder, A., Thew, M., & Harrison, D. (1998). A numerical investigation of solid particle erosion experienced

within oilfield control valves. *Wear*, *216*(2), 184–193. https://doi.org/10.1016/S0043-1648(97)00217-2

Goodwin, J. E., Sage, W., & Tilly, G. P. (1969). Study of erosion by solid particles. *Proceedings of the Institution of Mechanical Engineers*, *184*(1), 279–292. https://doi.org/10.1243/PIME_PROC_1969_184_024_02

Grant, G., & Tabakoff, W. (1975). Erosion prediction in turbomachinery resulting from environmental solid particles. *Journal of Aircraft*, *12*(5), 471–478. https://doi.org/10.2514/3.59826

Hua, H., Zeng, Y. Z., Wang, H. Y., Ou, S. B., Zhang, Z. Z., & Liu, X. B. (2015). Numerical analysis of solid-liquid two-phase turbulent flow in Francis turbine runner with splitter blades in sandy water. *Advances in Mechanical Engineering*, *7*(3), 1–10. https://doi.org/10.1177/1687814015573821

Johansson, M. (2012). Evaluation of RANS turbulence models for the hydrodynamic analysis of an axisymmetric streamlined body with special consideration of the velocity distribution in the stern region.

Kang, M. W., Park, N., & Suh, S. H. (2016). Numerical study on sediment erosion of francis turbine with different operating conditions and sediment inflow rates. *Procedia Engineering*, *157*, 457–464. https://doi.org/10.1016/J.PROENG.2016.08.389

Karunarathne, S. S., & Tokheim, L. A. (2017). Comparison of the influence of drag models in CFD simulation of particle mixing and segregation in a rotating cylinder. 151–156. https://doi.org/10.3384/ecp17138151

Kaufmann, A. (2004). Towards the simulation of large scales in Euler-Euler formulation of two-phase reactive flows (Doctoral dissertation, Toulouse, INPT).

Klajbár, C., & Könözsy, L. (2016). Multiphase eulerian simulations of a sedimentation process in a solid-fluid particle-laden flow.

Koomullil, R., Soni, B., & Singh, R. (2008). A comprehensive generalized mesh system for CFD applications. *Mathematics and Computers in Simulation*, *78*(5–6), 605–617. https://doi.org/10.1016/j.matcom.2008.04.005

Li, Y., Zhang, H., Lin, Z., He, Z., Xiang, J., & Su, X. (2019). Relationship between wear formation and large-particle motion in a pipe bend. *Royal Society Open Science*, *6*(1), 181254. https://doi.org/10.1098/rsos.181254

Lote, D. A., Vinod, V., & Patwardhan, A. W. (2018). Comparison of models for drag and non-drag forces for gas-liquid two-phase bubbly flow. *Multiphase Science and Technology*, *30*(1), 31–76. https://doi.org/10.1615/MultScienTechn.2018025983

Mansouri, A., Arabnejad, H., Shirazi, S. A., & McLaury, B. S. (2015). A combined CFD/experimental methodology for erosion prediction. *Wear*, *332–333*, 1090–1097. https://doi.org/10.1016/J.wear.2014.11.025

Masoodi, J. H., & Harmain, G. A. (2017). Sediment erosion of Francis turbine runners in the Himalayan region of India. *International Journal on Hydropower and Dams*, 24, 82-89.

McLaury, B. A., Shirazi, S. A., Shadley, J. R., & Rybicki, E. F. (1995). Parameters affecting flow accelerated erosion and erosion-corrosion. *NACE International, Houston, TX (United States)*. https://www.osti.gov/biblio/106121

Morsi, S. A., & Alexander, A. J. (1972). An investigation of particle trajectories in two-phase flow systems. *Journal of Fluid Mechanics*, *55*(02), 193. https://doi.org/10.1017/S0022112072001806

Neopane, H. P., Dahlhaug, O. G., & Cervantes, M. J. (2012). The effect of sediment characteristics for predicting erosion on Francis turbines blades. *International Journal on Hydropower and Dams, 19*(1), 79-83.

Oka, Y. I., Okamura, K., & Yoshida, T. (2005). Practical estimation of erosion damage caused by solid particle impact: Part 1: Effects of impact parameters on a predictive equation. *Wear*, *259*(1–6), 95–101. https://doi.org/10.1016/J.wear.2005.01.039

Padhy, M. K., & Saini, R. P. (2008). A review on silt erosion in hydro turbines. *Renewable and Sustainable Energy Reviews, 12*(7), 1974–1987. https://doi.org/10.1016/j.rser.2007.01.025

Peng, W., & Cao, X. (2016). Numerical simulation of solid particle erosion in pipe bends for liquid-solid flow. *Powder Technology*, *294*, 266–279. https://doi.org/10.1016/j.powtec.2016.02.030

Pradhan, P. M. S. (2004). *Improving sediment handling in the Himalayas*. OSH research, Nepal, 1-6.

Prashar, G., Vasudev, H., & Thakur, L. (2020). Performance of different coating materials against slurry erosion failure in hydrodynamic turbines: A review. In Engineering Failure Analysis (Vol. 115). Elsevier Ltd. https://doi.org/10.1016/j.engfailanal.2020.104622

Rai, A. K., & Kumar, A. (2017). Sediment monitoring for hydro-abrasive erosion: A field study from Himalayas, India. *International Journal of Fluid Machinery and Systems, 10*(2), 146–153. https://doi.org/10.5293/IJFMS.2017.10.2.146

Rajkarnikar, B., Neopane, H. P., & Thapa, B. S. (2013). Development of rotating disc apparatus for test of sediment-induced erosion in francis runner blades. *Wear*, *306*(1–2), 119–125. https://doi.org/10.1016/j.wear.2013.07.011

Rakibuzzaman, M., Kim, H. H., Kim, K., Suh, S. H., & Kim, K. Y. (2019). Numerical study of sediment erosion

analysis in Francis turbine. *Sustainability (Switzerland)*, *11*(5). https://doi.org/10.3390/su11051423

Reichardt, H. (1951). Vollständige darstellung der turbulenten geschwindigkeitsverteilung in glatten leitungen. *ZAMM - Journal of Applied Mathematics and Mechanics / Zeitschrift Für Angewandte Mathematik Und Mechanik*, *31*(7), 208–219. https://doi.org/10.1002/zamm.19510310704

Sadrehaghighi, I., Smith, R., & Tiwari, S. (1992, January 6). *An analytical approach to grid sensitivity analysis*. 30th Aerospace Sciences Meeting and Exhibit. https://doi.org/10.2514/6.1992-660

Sangal, S., Singhal, M. K., & Saini, R. P. (2018). Hydro-abrasive erosion in hydro turbines: a review. In *International Journal of Green Energy, 15*(4), 232–253. https://doi.org/10.1080/15435075.2018.1431546

Shahsavari, A., & Akbari, M. (2018). Potential of solar energy in developing countries for reducing energy-related emissions. *Renewable and Sustainable Energy Reviews*, *90*, 275–291. https://doi.org/10.1016/j.rser.2018.03.065

Silva, R., Cotas, C., Garcia, F. A. P., Faia, P. M., & Rasteiro, M. G. (2015). Particle distribution studies in highly concentrated solid-liquid flows in pipe using the mixture model. *Procedia Engineering*, *102*, 1016–1025. https://doi.org/10.1016/j.proeng.2015.01.224

Singh, G., & Kumar, A. (2016). Performance evaluation of desilting basins of small hydropower projects. ISH Journal of Hydraulic Engineering, 22(2), 135–141. https://doi.org/10.1080/09715010.2015.1094750

Singh, M., Banerjee, J., Patel, P. L., & Tiwari, H. (2013). Effect of silt erosion on francis turbine: A case study of maneri bhali stage-II, Uttarakhand, India. *ISH Journal of Hydraulic Engineering*, *19*(1), 1–10. https://doi.org/10.1080/09715010.2012.738507

Singh, V., Kumar, S., & Mohapatra, S. K. (2019). Modeling of erosion wear of sand water slurry flow through pipe bend using CFD. *Journal of Applied Fluid Mechanics*, *12*(3), 679–687. https://doi.org/10.29252/jafm.12.03.29199

Teran, L. A., Roa, C. V., Muñoz-Cubillos, J., Aponte, R. D., Valdes, J., Larrahondo, F., Rodríguez, S. A., & Coronado, J. J. (2016). Failure analysis of a run-of-the-river hydroelectric power plant. *Engineering Failure Analysis*, *68*, 87–100. https://doi.org/10.1016/j.engfailanal.2016.05.035

Thapa, B. S., Dahlhaug, O. G., & Thapa, B. (2015). Sediment erosion in hydro turbines and its effect on the flow around guide vanes of Francis turbine. *Renewable and Sustainable Energy Reviews*, *49*, 1100–1113. https://doi.org/10.1016/J.RSER.2015.04.178

Thapa, B. S., Thapa, B., Eltvik, M., Gjosater, K., & Dahlhaug, O. G. (2012). *Optimizing runner blade profile of Francis turbine to minimize sediment erosion.* IOP Conference Series: Earth and Environmental Science, 15(PART 3). https://doi.org/10.1088/1755-1315/15/3/032052

Truscott, G. F. (1972). A literature survey on abrasive wear in hydraulic machinery. *Wear*, *20*(1), 29–50. https://doi.org/10.1016/0043-1648(72)90285-2

Vieira, R. E., Mansouri, A., McLaury, B. S., & Shirazi, S. A. (2016). Experimental and computational study of erosion in elbows due to sand particles in air flow. *Powder Technology*, *288*, 339–353. https://doi.org/10.1016/J.Powtec.2015.11.028

Zhang, Y., Reuterfors, E. P., McLaury, B. S., Shirazi, S. A., & Rybicki, E. F. (2007). Comparison of computed and measured particle velocities and erosion in water and air flows. *Wear*, *263*(1–6), 330–338. https://doi.org/10.1016/J.wear.2006.12.048

Zolfagharnasab, M. H., Salimi, M., Zolfagharnasab, H., Alimoradi, H., Shams, M., & Aghanajafi, C. (2021). A novel numerical investigation of erosion wear over various 90-degree elbow duct sections. *Powder Technology*, *380*, 1–17. https://doi.org/10.1016/j.powtec.2020.11.059